BULLETIN OF THE POLISH ACADEMY OF SCIENCES
TECHNICAL SCIENCES, Vol. 59, No. 3, 2011
DOI: 10.2478/v10175-011-0042-x

Microscale interpretation of tribological phenomena in Ti/TiN soft-hard multilayer coatings on soft austenite steel substrates

J.M. LACKNER[1], L. MAJOR[2*], and M. KOT[3]

[1] Institute for Surface Technologies and Photonics, Joanneum Research Forschungsges.m.b.H., Functional Surfaces, Leobner Straße 94, A-8712 Niklasdorf, Austria
[2] Institute of Metallurgy and Materials Sciences, Polish Academy of Sciences, IMIM-PAN, 25 Reymonta St., 30-059 Cracow, Poland
[3] University of Science and Technology, AGH, 30 Adama Mickiewicza Av., 30-059 Cracow, Poland

Abstract. The mechanical and tribological behavior of physical vapor deposited coatings on soft substrate materials gains increasing interest due to economical and environmental aspects – e.g. substitution of steels by light-weight metals or polymers in transport vehicles. Nevertheless, such soft materials require surface protection against wear in tribological contacts. Single layer hard coatings deposited at room temperature are brittle with a relatively poor adhesion. Therefore, they should be better substituted by tough multilayer coatings of soft-hard material combinations. However, the mechanics of such multilayer coatings with several 10 nm thick bilayer periods is difficult and yet not well described. The presented work tries to fill the gap of knowledge by focusing both on mechanical investigations of hardness, adhesion, and wear and on microscopic elucidation of deformation mechanisms. In the paper 1 μm thick Ti/TiN multilayer stacks were deposited by magnetron sputtering on soft austenitic steel substrates at room temperature to prevent distortion of functional components in future applications. High hardness was found for 8 and 16 bilayer films with modulation ratio Ti:TiN = 1:2 and 1:4. This was attributed (with use of transmission electron microscopy) to stopping the crack propagation in thin Ti layers of the multilayer systems by shear deformation combined with different fracture mechanisms in comparison with that for the TiN single layers (edge cracks at the border of the contact area and ring cracks outside, respectively).

Key words: Ti/TiN multilayer coating, magnetron sputtering, wear, TEM.

1. Introduction

Future technical solutions for tribology-related engineering applications in a tool industry and highly-stressed components for instance in automotive or aircraft industries require development of new multifunctional thin film materials providing superior mechanical, tribological, chemical and high-temperature performance. Concepts with proven high potential for the design of such novel coatings are based on nanocomposites and multilayer coatings with tailored properties [1–4]. The most versatile properties are offered by multilayer coatings, which allow control of properties in individual constituent layers by their chemical composition and (micro-)structure, and of the whole multilayer coating by the number of layers, thickness and order of their deposition [5–12]. In many tribological contact conditions, coatings comprising hard/soft (or repeated high/low elastic modulus) layers can offer much improved tribological properties compared to single-layered hard coatings [13–16]. Titanium (Ti)/titanium nitride (TiN) multilayer coatings may provide such properties. Ti interlayers and microlaminated Ti/TiN composites (multilayers) accommodate stresses and allow thicker composite coatings to be produced, with a significant improvement in toughness, adhesion and impact resistance and reduction in steady-state friction [17–19]. Thin Ti layers and high Ti:TiN ratios were shown to drastically reduce wear [20]. Such coatings are generally deposited by physical vapour deposition (PVD) techniques like magnetron sputtering, ion beam assisted deposition, arc evaporation, and pulsed laser deposition. In technical application, Ti/TiN multilayer coatings on cast iron piston rings relaxed interface stress and improved combustion engine performance [21]. During mechanical loading, brittle ceramic single layer coatings like TiN would crack under the bending stresses generated by elastic or plastic deformation of subjacent soft substrates, because thin coatings offer little resistance against bulk surface deflections. The thicker the coating on a deformable substrate, the higher the bending stresses are. This is the reason, why thick hard coatings would not fulfill the task of the tribological protection of soft substrate materials. By alternating hard and soft materials, the hard layers can effectively slide over each other, and this prevents the build-up of high-bending stress [22–25]. The 'soft' metal layers act as shear zones to permit sliding. Furthermore, internal interfaces can act as sites for energy dissipation and crack deflection [24, 25]. In conclusion, multilayer coatings with such alternating properties can combine high hardness with ability to deformation. Detailed studies of deformation mechanisms of multilayer coatings for high-resolution cross-sectional ob-

*e-mail: nmlmajor@imim-pan.krakow.pl

servations are still very rare owing to the complexity of necessary cross-section thin foil preparation. Reasonably, this work focuses on the micro- and nanoscale investigation of deformation in multilayer coatings on the model system Ti/TiN. The high-resolution transmission electron microscopy (HR-TEM) is used to visualize plastic deformation and cracking beyond and around hardness indents, scratching tracks, and slide wear tracks. Finite element modeling completes the frame of performed studies and is used for a detailed explanation of experimental results.

2. Experiments

2.1. Deposition. Magnetron sputtering was used to deposit 1 μm thick Ti and TiN single layered coatings as well as Ti-TiN multilayers with:

1. modulation (bilayer) periods of 31, 62, 125, 250 and 500 nm (totally 32, 16, 8, 4, and 2 bilayers, respectively) and Ti:TiN modulation ratio of 1:1, as well as
2. bilayer period of 125 nm (8 bilayers) and modulation ratio of 1:2 and 1:4. Before mounting the mirror-polished austenitic steel samples (DIN 1.4301) on the substrate holder in 100 mm distance and pumping down the equipment [26] to 1×10^{-5} mbar start pressure, all substrates were ultrasonically cleaned in acetone and ethanol. A second cleaning and surface activation step after pumping was carried out in anode layer source O_2-Ar plasma. The subsequent DC sputter deposition from pure titanium targets (grade 2) occurred on continuously rotated, -50 V biased substrates in pure Ar atmosphere for Ti layers and N_2-Ar mixtures for TiN layers, respectively, under a total pressure 3×10^{-3} mbar. Deposition conditions required for preventing substrate distortion in future industrial application were reached by deposition without substrate heating. To raise the TiN single layer adhesion, we used a thin Ti interface layer.

2.2. Film characterization. Mechanical and tribological testing. Indentations and scratch tests were done on a MCT-CSM Instruments tester. For each coating-substrate system, hardness measurements were performed with a Vickers diamond under 10 mN maximum load. The indentation results were afterwards analyzed using Oliver and Pharr theory [27] in order to get hardness (H) and elastic modulus based on Eqs. (1) and (2)

$$H = \frac{F_{\max}}{A_c}, \tag{1}$$

$$E_z = \frac{\sqrt{\pi}}{2}\frac{S}{\sqrt{A_c}} \tag{2}$$

with maximum load (F), contact area (A_C,) contact stiffness (S) and reduced elastic modulus (E_z). E_z was calculated based on Eq. (3):

$$\frac{1}{E_z} = \frac{1-\nu_i^2}{E_i} + \frac{1-\nu_m^2}{E_m} \tag{3}$$

with elastic modulus (E) and poisson number (ν). Subscripts i and m denote indenter and tested material, respectively. The diamond indenter was calibrated on fused silica sample for finding an accurate relation between contact area (A_c) and contact depth (hc) $A_c = G(hc)$ [28]. At least 6 indentations were done for statistics. For indentation experiments at higher force (max. 500 mN) a cone-shaped diamond indenter with a spherical tip (tip radius 20 μm) was applied to achieve fracture of the single and multilayer coatings. These indentations were used for calculating stress – strain curves of the coating-substrate composite and for analyzing the deformation and fracture behavior in TEM investigations. Toughness and adhesion of coatings were evaluated by scratch technique using Rockwell C diamond with 0.2 mm tip radius. During tests the load was rising linearly from 0.01 to 30 N at a 5 mm scratch length and at a linear speed of 5 mm/min. For all tested samples three scratches were done. Critical loads were determined after tests by optical observations of scratch tracks and from recorded acoustic emission and friction force signals. Critical loads LC1 and LC2 indicate loads when first cohesive and adhesive cracks appeared, respectively. Wear tests were performed on a ball-on-disc tribometer using 1 mm diameter Al_2O_3 balls. Tests were carried out within 2000 cycles and 1 N load. The wear index was evaluated after calculation of an integral of the removed material from wear track profiles by Eq. (4)

$$W_V = \frac{V}{P \cdot l} \quad \left[\frac{\text{mm}^3}{\text{Nm}}\right] \tag{4}$$

with volume of removed material (V), normal load (P) and length of the wear track (l).

Structural investigations and microscopy. The microstructure and deformation behavior of coatings were analyzed by application of transmission electron microscopy (TEM) (TECNAI G^2 F20 (200 kV FEG)) in bright field (BF) and high resolution (HR-TEM) techniques. Electron diffraction patterns and high resolution (HR) techniques were applied for phase analysis, energy dispersive X-Ray (EDS) and electron energy loss spectroscopy (EELS) for quantitative and qualitative chemical analysis. Thin foils for TEM investigations were prepared by focused ion beam technique (FIB) with gallium ions for milling (Quanta 200 3D DualBeam microscope equipped with in-situ OmniProbe micro- manipulator).

2.3. Simulation. The indentation of a spherical indenter with 20 μm tip radius into single and multilayer coatings was modeled by a finite element method (FEM, Ansys) (Fig. 1a). This method allows us to calculate deformation and stress fields (stress concentrations) [29–31] including plastic deformation of substrates which is impossible by applying only extended Hertz theory for coating-substrate systems [32, 33]. In our models the mesh was densified close to the contact zone to the indenter, where significant stress concentration was expected (Fig. 1b).

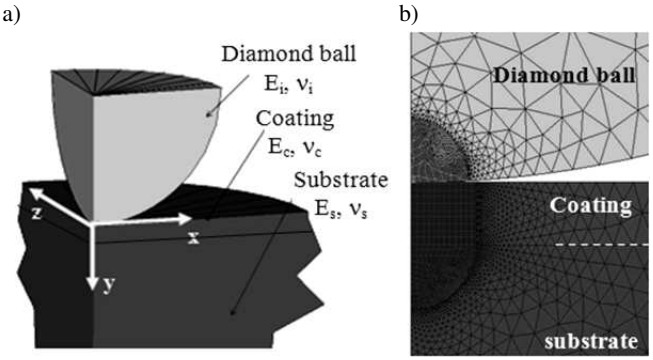

Fig. 1. Schematics of the modelled indentation in the coating-substrate system: a) view 1/4 of the model, b) finite elements mesh

We assumed perfect adhesion of the coatings to the substrate surface and between all sublayers in multilayer coatings. Coefficient of friction (μ) between indenter and coating was fixed at 0.1, which was experimentally found in scratch tests under a low load. The mechanical properties of coatings and substrate were adopted from indentation results. TiN were assumed as perfectly elastic, whereas perfectly plastic mechanical behavior was adopted for Ti layers. All systems were modeled without contribution of residual stress, because of problems with residual stress measurements for multilayers. Distributions of von Mises stress were analyzed leading to plastic deformation of substrates and first principal stress (tensile) responsible for coatings fracture [34, 35].

3. Theoretical aspects in single vs. multilayer deformation – FE simulations

For understanding the improvements of using of soft-hard multilayer coatings we will first focus on the deformation of a system consisting of a hard, brittle single layer (thickness d) on a thick compliant substrate, being indented with the force (P) over a radius (a) at the top surface [36] (Fig. 2). The assumption of a fixed (nonzero) contact area ensures elastic deformation up to a critical load for fracture ("blunt" contact [37]), thereby simplifying the analysis. Three regions of relative thickness (d/a) can be identified (Fig. 2):

1. Thick coatings (Fig. 2a): The system behaves as a brittle monolith, with the stresses concentrated at the top surface. Fracture occurs as a near-axisymmetric cone crack close to the contact circle, where the tensile stresses are maximum [38].
2. Thin coatings (Fig. 2b): The coating begins to flex, and the primary maximum in tensile stress shifts to the coating lower surface [39]. Radial cracks initiate in the center region and propagate on median planes through the contact axis. At the top surface, the peak tensile stress moves outwards from the contact circle onto the shoulders, forming relatively shallow, secondary ring cracks.
3. Thin films (Fig. 2c): Cracking becomes suppressed within the compression zone beneath the Hertzian contact, and the maximum tensile stresses shift back to the top surface close to the contact circle [39–41]. Membrane stresses come increasingly into play. Although detailed fracture mechanics descriptions for all three regions are complex [38], conservative relations can be obtained by considering fracture to occur when the tensile Hertzian stresses in region (1), the flexural (bending) stresses in region (2) or thin film tensile stresses exceed coating strength [42].

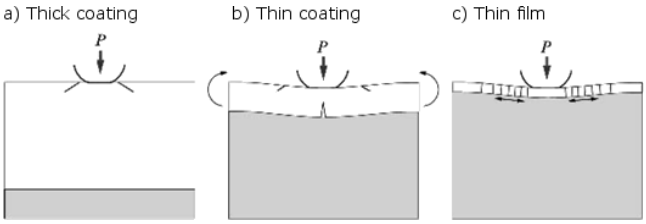

Fig. 2. Schematics of bilayer structure and deformation/fracture regimes of a brittle layer on a thick compliant substrate under axisymmetric indentation. a) Thick coatings: cone crack at top surface, b) thin coatings: ring crack at the top surface, c) thin films: concentric through-thickness ring cracks (after Ref. [36])

Diminishing substrate deformation would increase resistance to coating fracture in regimes (2) and (3), which are of main interest for PVD coatings. This is feasible only by the coating material or material combination: (I) by increasing the "elastic strain to failure", which is related to a high value of the ratio H/E [43, 44], or (II) by decreasing the bending stresses in the hard layer. While option (I) is fulfilled by the concept of nanocomposites coatings, option (II) results in multilayer coatings, in which the thickness of the single hard layer is drastically decreased by introducing soft layers, on which the hard layer can effectively slide relative to the layers below. This attempt follows the well-known bending stress formula (Eq. (5)), underlining that a thick hard coating (half thickness z) will see higher bending stress compared to thin coatings, when bent to the same radius.

$$\sigma = -\frac{M_b}{I_y} z \tag{5}$$

with bending moment (M_b) and axial moment of area (I_y). The purpose of the softer and, thus, lower elastic modulus layers is therefore the accommodation of relative sliding (shear strains) of the hard layers below and above [23, 45–47]. If the cohesion strength in one of the thin brittle layers in the multilayer, stack is exceeded, cracking will first only bridge through this layer in between the two soft deformable layers and would not obligatory pass the whole coating thickness. Reasonably, this effect is highly comparable to fracture mode (3) (Fig. 2c).

To discuss the multilayer effect based on stresses occurring during indentation of a spherical indenter, we modeled both a TiN single layer and a multilayer consisting of 4 bilayers (Ti + TiN), both 1 μm thick, on austenite substrate (data from DIN 1.4301). The results, shown in Fig. 3 and 4, reveal differences in the deformation behavior of these two systems in the elastic and plastic regime:

– In the elastic regime (P = 2 mN), shown in Figs. 3 and 4a, distribution of the first principal stresses attains a max-

imum value at the surfaces of both single and multilayer coatings (Fig. 3a and b, respectively) outside the contact region as expected for thin coatings from the three modes shown in Fig. 2b. This is in accordance to literature of multilayer stress simulation [48], which defines cracking either on the multilayer surface or in the hard phase at one of the interfaces close to the surface, depending on the contact geometry (ratio coating thickness to indenter tip radius). Figure 4a shows stress distribution calculations of the maximum principal stress on the coating surface in single layer coatings or close to the interface in multilayer coatings, normalized to the average value of contact pressure in the contact zone. Lower tensile stresses in the elastic regime and lower deformation ("SL-TiN-P.depth", "M8-P.depth") are found for the stiffer single layer (lower composite elastic modulus). The maxima are found on the surface outside the contact area ("SL-TiN top" for the single layer coating and "M8-Top" for the multilayer coating), while on the interface of the single layer to the austenite substrate ("SL-TiN Int") and the TiN layer closest to the substrate ("M8-Bot") highest stresses occur on the symmetric axis.

– In the fully developed plastic deformation regime (P = 200 mN) maximum stresses arise in similar areas as for the elastic regime (Fig. 4b), but the first principal stresses both at the coating surface and the interface are higher than the mean pressure (pm) in the contact area ($\sigma 1/pm = 1.9$ and 1.35 (plastic) vs. 0.12 and 0.15 (elastic) for single and multilayer coatings, respectively). Most important are the developing higher principal tensile stresses for the multilayer coatings, which are connected to the lower deformation compared to the single layer coatings. The large expansion of the deformation region in the multilayer results in less bending at the border of the contact zone and, thus, lower bending stresses. This all is due to the plastic deformation (shear) in the soft Ti layers.

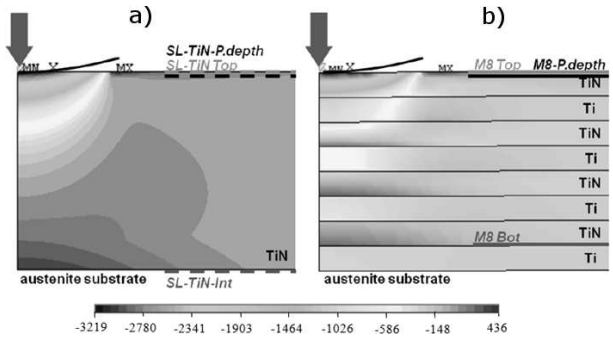

Fig. 3. FEM simulation of the first principal stress ($\sigma 1$) in (a) a TiN single layer coating and (b) a multilayer coating consisting of 4 bilayers (Ti + TiN) with modulation ratio Ti:TiN = 1 on austenite steel substrate in the elastic regime (P = 2 mN). Abbreviations are given for explanation of Fig. 4

In conclusion, this model calculation explains, why the combination of soft-hard bilayers in multilayer coatings reduce the local deformation and bending stresses by increasing the deformed area and volume.

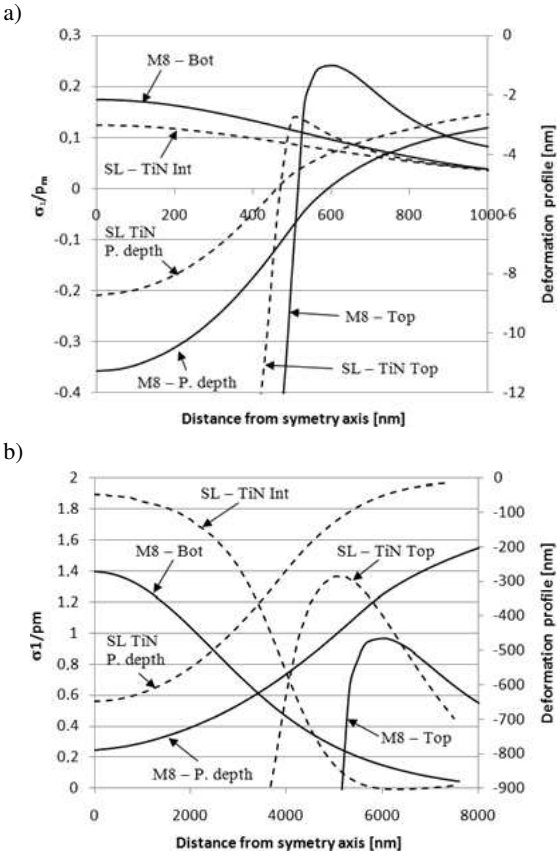

Fig. 4. Coating surface deformation and the first principal stress in the single TiN layer and in Ti + TiN multilayer coating as a function of the distance from the axis of symmetry for the (a) elastic regime (P = 2 mN) and (b) fully developed plastic regime (P = 200 mN). All stresses are normalized to an average value of the contact pressure $\sigma 1$/pm in the contact zone. Abbreviations for location of stress and deformation graphs in the FE model can be taken from Fig. 3

4. Results and discussion

4.1. Microstructure and nanostructure of coatings. The thin ceramic PVD coating deposited at low temperatures are generally characterized by columnar structure with microcracks, pinholes, transient grain boundaries and often a high degree of through-coating porosity. In the Thornton structure model [49] "Zone 1" is merged at higher ion bombardment during deposition to a transition "Zone T" consisting of fibrous grains a highly decreased porosity. The enhanced surface diffusion during deposition with higher energetic particles fills the gaps between the columns and increases the cohesion strength of the coating. Presented coatings were manufactured at the transition from Zone 1 to Zone T, as shown in Fig. 5 for a TiN single layer.

Due to high compressive residual stress in the single layer TiN coating, microcrack-like features are forming along the column boundaries. In high-resolution images (Fig. 5c), they consist of accumulation and pile-up of dislocations between the columns. According to literature, microcracks are nucleated in crystalline materials by three different mechanisms: dislocation pile-ups, twin intersections, and strain incompatibility [50]. Thus, the found features are nucleation sites for

evolving microcracks. In previous investigations of stress of similar type of coatings, deposited by PLD [19], we found compressive intrinsic stresses of up to 12 GPa for 1 μm thick single layer TiN films, which diminish to 3.5 GPa for TiN in 32 bilayer films. Thus, crack formation can start even without external loading by e.g. stress relaxation mechanisms, as described e.g. for polymers in [51]. (Ti/TiN) multilayer coatings are characterized by much finer columnar microstructure and smaller or missing microcracks as visible in Fig. 6. Because intrinsic stresses are generally responsible for their formation, this can be explained by the lower stress level in these films. Additionally, the sequence of soft-hard materials with easy shearing and crack propagation stop at the interface prevents also large fractures (see below).

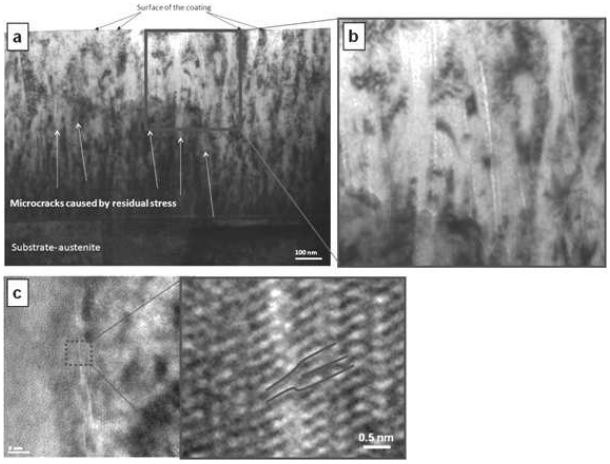

Fig. 5. TEM bright field cross-section images of TiN single layer films. (a) image of the whole thickness, (b) TEM and (c) HR-TEM details of microcrack-like features in the coating

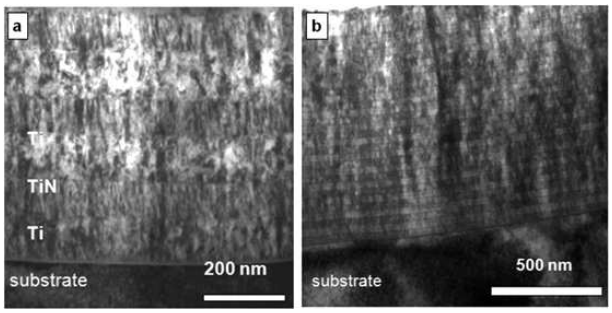

Fig. 6. Bright field, cross section TEM images of multilayer coatings: a) 4 bilayers and b) 16 bilayers (Ti/ TiN)

Figure 7a reveals similar type of diffraction contrast in the micro-columns across the interfaces in the multilayer indicating crystallographic dependence between the individual layers. In Fig. 7b it can be traced by the change from Ti [0 0 1] to TiN [1 1 0] zone at the interface with slight change of lattice orientation from 60° to 70° between (1 0 0)/(0 1 0) Ti and (1 −1 1)/ (1 −1 −1) planes in the TiN. Some crystallites from the metal phase pass the interface to the ceramic face and ceramic crystallites to metallic phase.

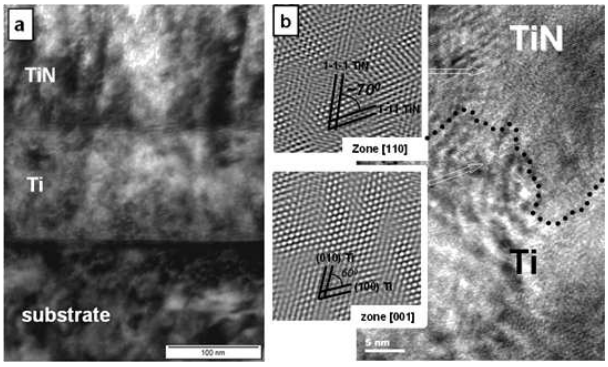

Fig. 7. Bright field, cross section (a) TEM image of the interfaces austenite steel – Ti and Ti/TiN in the multilayer coating with 8 bilayers and (b) HR-TEM image of a Ti-TiN interface in the multilayer coating with 16 bilayers with indicated lattice orientations

4.2. Deformation of coatings under static point loads – deformation phenomena in hardness testing. Quantification of mechanical properties under low loads with Vickers indentation. The hardness of all coatings in Vickers indentation testing with 10 mN maximum load was found to be highly dependent on the modulation (bilayer) period (Fig. 8a) and modulation ratio TiN:Ti (Fig. 8b). Compared to the rule of mixture (RM) (Eq. (6))

$$H_{\mathrm{RM}} = \frac{t_{\mathrm{Ti}}}{\lambda} \cdot H_{\mathrm{Ti}} + \frac{t_{\mathrm{TiN}}}{\lambda} \cdot H_{\mathrm{TiN}} \tag{6}$$

it reveals higher hardness for medium bilayer periods. In this equation H_{RM} is the hardness resulting from the rule of mixture, H_{Ti} and H_{TiN} the hardness of Ti and TiN single layer coatings, t_{Ti} and t_{TiN} the thickness of Ti and TiN sublayers, respectively, and $\_ = t_{\mathrm{Ti}} + t_{\mathrm{TiN}}$ the bilayer period. Decreasing the bilayer period raises the hardness; the highest hardness (23.8 GPa) was measured for 16 bilayer coatings ($\lambda = 62$ nm), while the increase to 32 bilayers causes a drastic drop towards the RM hardness. This behavior is similar to many results presented in literature (e.g. [52–61]) with an optimal bilayer thickness to be dependent on the material combination. The increase of hardness with decreasing bilayer period is attributed to Hall-Petch strengthening [62], which originally relates yield strength to the dislocation pileup at grain boundaries. Its modification for multilayer coatings states, that layer interfaces are barriers for dislocation motion necessary for plastic deformation (Eq. (7)),

$$H_{multi} = H_0 + \frac{k_{\mathrm{HP}}}{\lambda^{0.5}} \tag{7}$$

in which H_0 is the hardness for high bilayer periods (single layer coating) and k_{HP} is a constant fitted to the indentation results. Also the hardening model of Lehoczky [63] with the constant k_L fits well (Eq. (8)),

$$H_{multi} = H_0 + \frac{k_L}{\lambda} \tag{8}$$

which was developed in order to express the strengthening of multilayers due to resistance of dislocation flow across layers with different dislocation line energies (related to shear moduli). Based on these theories the decrease of hardness for the

32 bilayer coating is due to the loss of multilayer structure due to an increased number of defects on and near the interfaces.

Modulating the TiN:Ti ratio (Fig. 8b) (layer thickness of TiN to the one of Ti) for the 8 bilayer coating (125 nm total bilayer thickness) increases the multilayer hardness with increasing TiN content. The hardness of the multilayer coating for the TiN:Ti ratio equal to 4 is even higher than the hardness of TiN single layer coating, revealing no loss of hardness by introducing 25 nm thin, soft Ti interlayers. As expected by the Hall-Petch effect, the hardness is also higher than predicted by the role of mixture. Similar results were published also by other authors (e.g. [64, 65]).

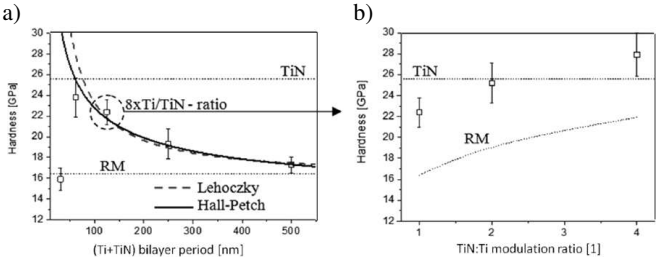

Fig. 8. Hardness of Ti/TiN multilayer coatings (a) as a function of modulation (bilayer) period at a modulation ratio TiN:Ti = 1:1 and (b) as a function of the modulation ratio TiN:Ti for 8 bilayer (Ti/TiN) coatings. For comparison well described theories for the rule of mixture (RM) and dislocation driven hardening mechanisms (Lohoczky and Hall-Petch) are given

The tribological performance is both dependent on hardness and elastic modulus. The elastic modulus of our films, calculated from the indentation curves, follows the rule of mixture for modulation ratio TiN:Ti = 1:1. While for 1 μm thick Ti and TiN single layers their elastic moduli were 163 and 380 GPa (respectively), elastic moduli for the multilayers are approximately constant (between 255 GPa and 268 GPa) for the number of bilayers less than 16 and slightly decreases to 240 GPa for 32 bilayer films. All these values are below the one calculated from the rule of mixture (271.5 GPa). For thicker TiN layers (e.g., for the modulation ratio TiN:Ti equal to 2:1 or 4:1 for 8 bilayer films), the measured elastic modulus is approximately constant as well ($\sim$275 GPa), which is much less than that expected from the rule of mixture. For the design purposes, the wear resistance can be predicted by the "elasticity index" H/E, describing the elastic strain to failure [43, 66]. Furthermore, this ratio is important for coatings: A coating which can deflect with the substrate's deformation under an applied load without fracture is vital, and this requires a high elastic strain to failure, i.e. a high H/E ratio [45]. Thus, the ratio is a measure of ability to absorb energy elastically. The resistance of a coated surface to plastic deformation is proportional to H^3/E^2 ("plasticity index"), because the yield pressure in a rigid ball contact during an elastic/plastic deformation is a function of this ratio [67, 68]. Both low elastic modulus and high hardness prevent plastic deformation. Finally, H^2/E defines the resistance to fracture (Irwin-Orowan-Griffith case) with the energy release rate (expressed by the elasticity modulus) proportional to the square of the critical stress to failure (expressed by the hardness). Tough materials are characterized by high H^2/E [69]. Examples of the H/E dependence on the bilayer period and modulation ratio are given in Fig. 9. Compared to soft single layers Ti and TiN with $H/E = 0.044$ and 0.067 (respectively) the elastic strain to failure is for all multilayer coatings higher, e.g. about 40% higher for the 16 bilayer coating with modulation TiN:Ti = 1:1 and 50% higher for the 8 bilayer coating with modulation 4:1. We received a similar curve shape for the plasticity index H^3/E^2 – describing the ability for plastic deformation or toughness – although only the 8 and16 bilayer coatings independently of the modulation ratio have higher H^3/E^2 than single TiN layer. Similar to H/E, the H^3/E^2 ratio increases with the high modulation ratio. The same trend is followed by H^2/E ratio, characterizing the resistance to fracture.

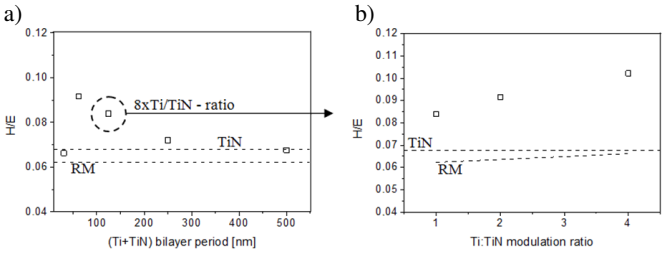

Fig. 9. Elasticity index H/E of Ti-TiN multilayer coatings (a) as a function of modulation (bilayer) period at a modulation ratio TiN:Ti = 1:1 and (b) as a function of the modulation ratio TiN:Ti for 8 bilayer (Ti+TiN) coatings

Quantification of mechanical properties under high loads with spherical indentation. High load indentation (500 mN maximum load) with spherical indenter (20 μm tip radius) resulted in penetration depths of 1700 to 2000 nm, which is up to 2 times higher than the coating thickness. Such high point loadings triggers deformation and coating fracture. The cracks formed in single layer TiN (Fig. 10a) are ring cracks around the indent (compare to [70, 71]) and spread from the surface at the periphery of the contact area through the coating thickness towards the substrate (as revealed later). Additionally, we found lateral, nestled cracks beneath the deformation zone parallel to the surface or at the interface coating/substrate, but radial cracks starting from the indent circumference (e.g. edges in Vickers' indents) are missing for the spherical indenter geometry. For the multilayer coating of 8 bilayers and modulation ratio equal to 1 (Fig. 10b) cracking is rather not visible in the light microscopy images. Increasing the modulation ratio TiN/Ti to 2 or 4 as well as the number of bilayers to 16 or 32, does not change this behaviour. However, the 2 and 4 bilayer coatings show ring cracks of a decreasing intensity. Taking in account the discussion of the hardness to elastic modulus ratios above, the tendency of fracture can easily be correlated to elasticity and / or plasticity index. Before the appearance of large cracks, hard coatings yield local cracking at the range of nano and micrometer length scales. This is accompanied by the formation of kink-like and zigzag discontinuities (pop-ins) on the load-displacement curve as shown

in Fig. 10c for TiN single layer coatings. When a ductile material such as austenitic stainless steel was indented under the same conditions, smooth load-displacement curves were obtained, leading us to correlate load-curve discontinuities to the deformation processes in hard films under Lackner et al. 14 indentation load. Similar smooth curves were found for our multilayer coatings. The small scale discontinuities in our load-displacement curves appear from the beginning of the loading period, but become more and more pronounced beyond a certain displacement of the indenter (150 mN). While under lower loads an opening of existing microcracks (see Fig. 5) is expected for the brittle TiN single layer to adapt to the indenter and deforming substrate geometry, the larger pop-ins seems to originate in substrate formation beyond the coating [72] due to the inability of hard materials to sustain large plastic straining. Missing pop-ins for the multilayer coatings can be easily correlated to the surface impression around and in the indents with missing visible cracks.

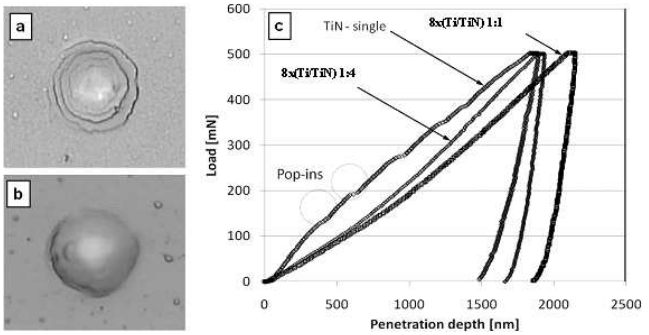

Fig. 10. High load (500 mN) indentation with spherical indenter. Light microscopy images of the crack patterns of a 1 μm thick TiN single layer (a) and a 8 bilayer coating with TiN:Ti modulation ratio 1:1 (b), both on austenite steel; (c) Indentation curves for single layer TiN and two 8-bilayer (TiN/Ti)×8 coatings with modulation ratios TiN:Ti equal to 1 and to 4 (respectively)

Indentation curves were transformed into stress-strain curves (Fig. 11) following a procedure based on determination of contact stress pm $= P/$Acont (with force P and real contact area Acont) and strain $\varepsilon = a/Ri$ (with contact radius a) in indentation experiments under various loads [73, 74]. For TiN single layer coating a higher stress level (mean pressure) was found. When strain reaches $\varepsilon = 0.14$ at pm $= 4$ GPa, a drop of stress was observed, which corresponds to first pop-in under 150 mN load. Thus, the stiffer single layer coating is severely fractured by ring cracking around the indenter, while the substrate deforms plastically further on – visible by the step-wise decrease of contact stress after the maximum. A slightly lower initial slope of the stress-strain curve in the "elastic regime" was found for multilayer coatings, resulting from higher contact area and a lower mean stress (compare the results of the FEM simulation). The stable stress level (pm $= 2.5$ GPa) starting at $\varepsilon = 0.07$ reveals deformation controlled by continuous plastic substrate deformation with minor coating fracture.

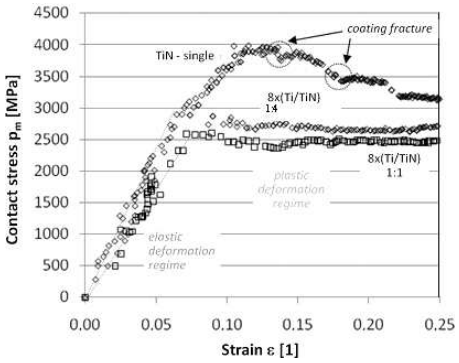

Fig. 11. Stress-strain curves calculated from spherical indentation curves of single layer TiN and 8 bilayer coatings with modulation ratio TiN:Ti = 1:1 and 4:1, respectively

Micron scale deformation and microstructure analysis of the coatings after indentation tests at high loads with spherical indenter. For the investigations of deformation and microstructure changes in micro- and nano-scale we used the same indents from spherical indentation as used above for the stress-strain curve calculation. Thin foils from the axis of symmetry were prepared and investigated in TEM. Evaluation of deformation and cracking in 1 μm TiN single layered coatings are shown in Fig. 12. During the indentation with spherical indenters (20 μm tip radius) the coating is initially compressed in normal direction, but as soon as the indentation contact pressure reaches the low yield stress of the austenite substrate it behaves like a perfectly elastic medium, transferring the indentation load directly to the substrate, which in turn deforms plastically (Fig. 12a). Both the extensive plastic deformation of the substrate and the inability of the coating to accommodate such deformation during loading lead to a concentration of tensile radial stresses at the coating-substrate interface just below the indenter (according to [72] and as found in FEM analysis described above). Their release occurs by brittle crack propagation towards the surface at the columnar grain boundaries due to the shear sliding of adjacent columns under indentation edges (nestled cracking in Fig. 12d). This process also minimizes the shear loading. The crack tips close near the top surface of the impression as the propagation approaches the zone of compression. This process might be particularly effective for strain energy dissipation, hence avoiding premature failure by delamination of the coating along the interface with the substrate. The visible, 50 nm thin Ti interface preventing delamination from the substrate is compressed too, shears parallel to the substrate surface ("thinning") and intensifies nestled cracking below the indenter (Fig. 12d). Major cracking is present outside the indenter contact area too (Fig. 12b) in high tensile stress regions (maximum first principal stress according the FEM simulation). The occurring ring cracks (compare to the light microscopy image in Fig. 10a) pass almost the full TiN coating thickness, as visible in Fig. 12b. Both the described fracture types belong to intercolumnar cracking, most probably following the paths of the still existing micro cracks in the as-deposited, non-deformed material. Shear cracks parallel to the interface (Fig. 12c) give hints to high shear stresses at the cir-

cumference region of the indenter contact. These lateral cracks are thought to probably originate on unloading of the indentation cycle and tend to propagate approximately parallel to the interface, releasing the elastic strain energy stored during bending [72]. Plastic deformation before cracking in TiN single crystals was studied by several authors in the past [76, 77]. The primary slip system for dislocation glide in TiN with ionic B1 NaCl crystal structure has been characterized by plastic deformation on $\{1\ 1\ 0\}$ planes with slip occurring along the $<1\ 1\ 0>$ directions corresponding to the shortest distance between either two cations or anions [72].

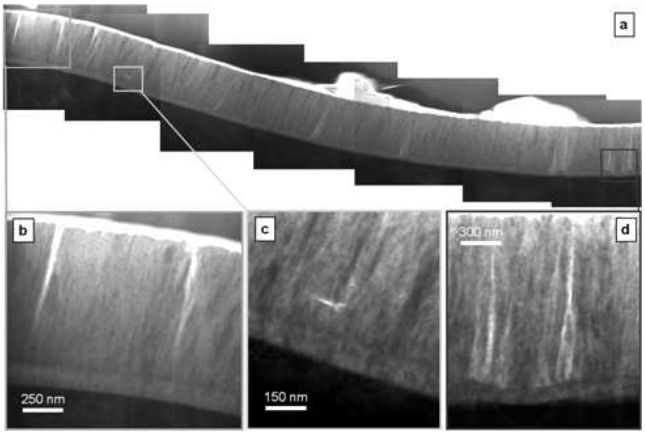

Fig. 12. (a) Deformation of 1 μm thick TiN single layer coating on austenite substrate by a 20 μm tip radius spherical indenter under 500 mN force. Details are showing (b) ring cracks outside, (c) shear cracks at the border of, and (d) nestled cracks in the centre of the contact area

In Ti/TiN multilayer coatings no cracks are visible on the surface, as shown in Fig. 9. TEM investigations (Fig. 13) reveal only cracking at the border of the contact area in a similar position as the shear cracks in TiN single layer coatings. Nestled cracks and ring cracks are missing. Focussing in detail on the cracking behaviour confirms the multilayer effect of stopping crack propagation at all interfaces (crack due to splitting or deflection) and deformation of the softer Ti layers [78]. For multilayers with modulation ratio TiN:Ti = 1:1 coating deformation appeared to be accommodated primarily by intergranular shear sliding and plastic flow of soft titanium layers. So called deformation lines (shear planes) are propagating across the coating at an angle of 45° to the surface, which is a typical angle for plastic deformation of polycrystalline metallic materials. Cracking occurs in the brittle TiN layers if the tensile stress is too high (Fig. 13b). The stress accumulation occurs mainly by Ti plastic deformation. An intercolumnar shear step, in which the above described phenomena occur, starts at the interface near the indentation contact edge, passing the whole coating thickness with an angle of about 55° to the surface (found for multilayer coatings also in [79]). The deformation seems to be highly focussed at the bottom close to the austenite substrate, which is due to the increasing contact area at higher loads, unloading (or compressive stressing) existing shear bands and, thus, forming stepwise several concentric bands. Varying the TiN:Ti modulation ratio to 2:1 (Fig. 14) results in similar deformation behave our, but with a shift of angular alignment of the shear band to $\sim 70°$ to the surface. Such behaviour can be explained by the increasing content of the hard TiN phase and as a result of the increasing fractured part of the coating. Similar behavior has been found for the multilayer coatings with TiN:Ti ratio equal to 4 (Fig. 15), which start to crack nearly perpendicular to the surface due to a very low content of the metal phase in the multilayer stack. Nevertheless, we noted an increase in elasticity and plasticity indices of the coating (H/E and H^3/E^2, respectively), calculated at low loads (10 mN), with increasing modulation ratio. The stress-strain curves, calculated at the same loads (500 mN), let to obtain similar deformation behaviour for TiN/Ti multilayers with the multilayer ratio 1:1 and 4:1. As a conclusion, toughness of the coatings is reasonably increasing even when plastic deformation is decreasing, because the crack stopping mechanisms by plastic deformation of Ti are not affected.

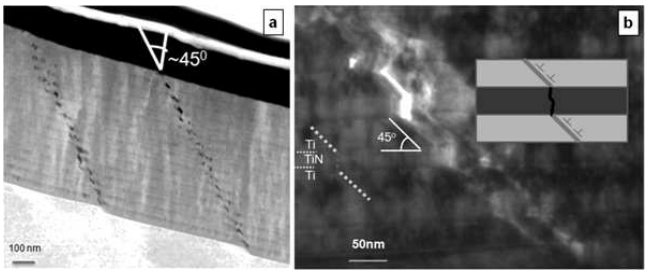

Fig. 13. Cross section TEM image of a 16 bilayer multilayer coating with modulation ratio TiN:Ti = 1:1. a) Overview and b) detail of deformation mechanisms (schematics of deformation and cracking)

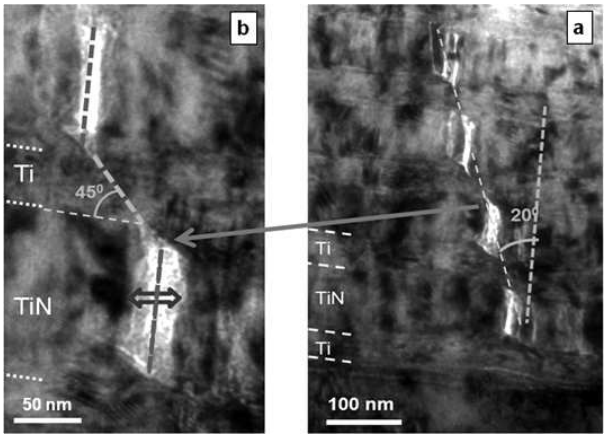

Fig. 14. Cross section TEM image of a 8 bilayer multilayer coating with modulation ratio TiN:Ti = 2:1. a) Overview and b) detail of deformation mechanisms

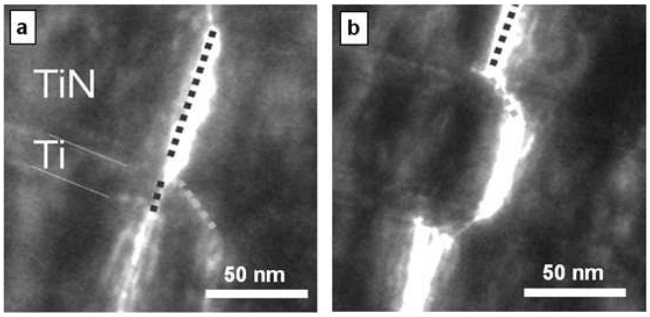

Fig. 15. Cross section TEM image of a 8 bilayer multilayer coating with modulation ratio TiN:Ti = 4:1. a) Overview and b) detail of deformation mechanisms

4.3. Deformation of coatings under dynamic point loads – deformation and fracture phenomena in scratch and wear testing. Single-pass sliding – scratch resistance and deformation. To show more obviously the difference between failure modes in multilayers as well as to assess fracture toughness and adhesion of films, scratch tests under continuously increasing loads were conducted. When a diamond indenter is drawn across the coating surface a range of possible failure modes can occur, depending on coating adhesion and cohesion. The critical loads for coating failure, LC1 and LC2, are determined on the basis of the first occurrence of cohesive failure (i.e., crack initiation within the coating) and adhesive one (i.e., coating detachment from the substrate) in the tracks, respectively (Table 1). After scratch testing, the surfaces were examined by light microscopy to identify the types of failure. For the TiN single layer coatings the first cohesive (non conformal) cracks were observed at a load of ~5 N, while further loading led up to LC2 = 13 N led to chipping on the lateral sides of the scratch track due to adhesive cracks, exposing the substrate. For multilayer coatings of the modulation ratio 1, the Lc1 increases only up to 8 bilayers (for greater number of sublayers a significant drop was found). A ratio 2:1 and 4:1 has no drastic effects on LC1, but boosts LC2 value nearly twice in comparison with that for the 8 bilayer 1:1 coating (from 16 N for the 1:1 modulation ratio to 28 N for the 4:1 ratio). 2, 4 and 8 bilayer coatings with 1:1 modulation ratio have slightly positive effect on LC2, while the 32 bilayer coating has a lower resistance to scratching. Similar results have been found in other papers as well: Ma et al. [80] found for Ti-TiN multilayers a maximum LC2 for an intermediate thickness of the Ti Interlayers (TiN:Ti ratio ~ 4:1), because such films can sufficiently promote energy absorption without ductile failure in the Ti layers. Even a TiN:Ti modulation ratio 2:1 was considered to be inadequate for mechanical applications due to an excessive amount of soft metal content, being responsible for spalling at low loads. Similar feature was verified for an Al/AlN multilayer stacks in [81] as well as for Cr/CrN multilayers in our work [58]. Considering the failure modes and relating them to the results obtained in indentation and TEM investigations (Subsec. 4.2), let us propose the following microstructure related deformation and fracture mechanisms. First cohesive cracks occur after elastic-plastic deformation of both single and multilayer coatings inside the scratch track under the spherical indenter. Increasing the load intensifies the ploughing effect due to compressive stresses in front of the indenter (vis. [70]). As a result irregular microcracks apper, which are flattened by the indenter and, due to that, not well visible in Fig. 16a (left side in any of the images). These stresses create bending and shearing, which can result in delamination (spalling) of the TiN single layer coating at quite low loads, as described above and shown in Fig. 16a. Multilayer coatings are more resistant to delamination from the substrate. In contrast, adhesive failure can occur at the Ti-TiN interfaces by shearing of Ti layers and cracking of the TiN ones. This failure is, however, not severe for 8 bilayer coatings with TiN:Ti multilayer ratio 1:1 (Fig. 16b). Increasing the TiN content (e.g., for a 2:1 or 4:1 ratio) results in a quite dense network of cracks in the scratch track, however, with no severe delamination from the substrate (Fig. 16c). First spalling was found for all multilayer coatings at the border of the track (Figs. 16c and d). This increasing resistance to scratch and spallation can be related to the decreasing metal content and a change of the fracture direction or of a deformation band angle from 55° to nearly perpendicular to the coating's surface. Fractured coating segments are more stable, if the fragments are notoverhanging above other, adhering coating fragments (for the multilayer ratio 1:1) but instead forming compact fragments (for the ratio 4:1).

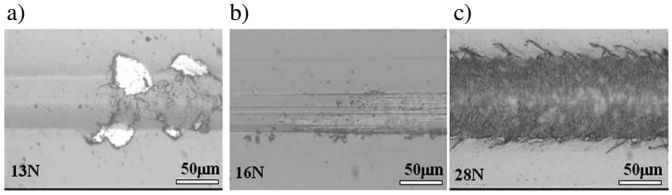

Fig. 16. a) Critical loads LC1 and LC2 for cohesive and adhesive coating failure, respectively, for TiN single layer and for Ti-TiN multilayer coatings with different bilayer periods and modulation ratios. Standard deviation for all measurements is below 5% of the measured values; b) Light microscopy image of a total failure for the scratch track at the critical load LC2 for TiN single layer coating; c) and d) – 8 bilayer multilayer coatings with modulation ratio TiN:Ti equal to 1 and to 4, respectively

Deformation and wear resistance during multi-pass sliding. Wear of a material is influenced by a number of parameters, of which the most important are its hardness and toughness as well as the coating's adhesion to the substrate and the fatigue resistance of the system coating/substrate (the latter is important in particular for a multi-pass sliding. The friction coefficient against alumina ball in the pin-on-disc experiments was found to be similar for TiN and all multilayer coatings except for the 32 bilayer stack. For the load 0.2 N, the friction coefficient is around 0.17–0.2, increasing to 0.19–0.22 for 1 N and 0.2–0.3 for 2 N, respectively. The highest values were found only for the 16 bilayer multilayers, while for all the other multilayers it was slightly lower (0.1–0.2) than for the single TiN layer. The wear resistance of the multilayer coatings with TiN:Ti modulation ratio 1:1 was slightly less than that for multilayers with high or medium values of the bilayer

periods and close to that for a single TiN layer (Fig. 17). As expected for low values of the hardness and adhesion strength, the tribological resistance of 32 bilayer coatings is low. Varying the modulation ratio to 2:1 and to 4:1 increases the wear resistance of the both coatings 5 times compared to corresponding values for the modulation ratio 1:1.

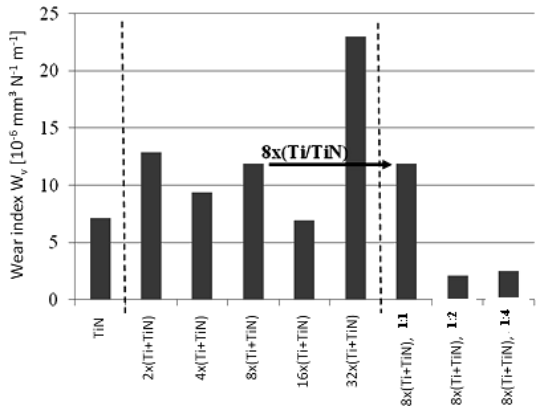

Fig. 17. Wear coefficient of single TiN layer and Ti-TiN multilayer coatings against alumina ball sliding in a pin-on-disc test

Explanation of such a wear behaviour during wear seems to be due to the toughening mechanism in multilayer films (related to their H/E ratio – see Subsec. 4.2.). Martinez et al. [82] and Berger et al. [57] found for hard substrates like silicon a layer by layer pin-on-disc wear of multilayer coatings, while same coatings on softer substrate materials (of much less load support) are subject to high substrate deformation and coating fracture during wear. Similar statement is valid for our films as well: TEM observations of the wear track for TiN single layers under low load (0.25 N) showed an abrasive wear in the wear track centre (Fig. 18a). This wear mode is a consequence of fatigue and intergranular cracking of the TiN coating surface region, revealed by the rough surface. The TiN coating is abraded by small surface asperities of the alumina ball acting as cutting edges and provoking sharp grooves in the film. Even under a relatively low load we found through-coating cracks due to a low resistance to deformation of both the austenite substrate (due to a plastic flow) and the TiN single layer coating (due to its fracture). Left and right of the main contact zone a tribofilm (or a transfer layer) is forming, consisting of Ti, N and O (Fig. 19). Material abraded from the centre of the wear track is oxidized and accumulates at the borders. Wear at higher loads (1 N) results even at low cycle number in fully fractured TiN single layer coatings in the centre of the wear track, while on the borders of the contact zone (Fig. 18b) dominates a through-thickness cracking and shear-step formation at the interface coating/substrate due to the substrate deformation and no continuous film survives in the centre. The tribolayers are formed both from the coating and and the substrate wear due to chipping and grooving. In contrast, the multilayer coatings can resist the scratching and grooving (Fig. 20a): wear occurs layer-by-layer, whereby the brittle TiN layers are – as expected – more wear resistant than the soft Ti ones. As an example, one can see the larger, only few nanometers thick titanium transfer layer on the TiN on the left side in Fig. 20a. A similar effect was found by Martinez et al. in [82]: in multilayers with high bilayer thickness (like in the 4 bilayer system shown in Fig. 20), the wear starts in the surface TiN layer until the fatigue cracks occur (triggered by the bending), which can propagate and reach the TiN-Ti interface (as shown in Fig. 20b). As a result, the TiN layer is delaminated and the Ti underlayer is quickly removed. If the TiN layers are very thin with a low content of the metal phase, no detachment of layers by fatigue cracking was observed. In contrast to that, a progressive wear of the coating took place.

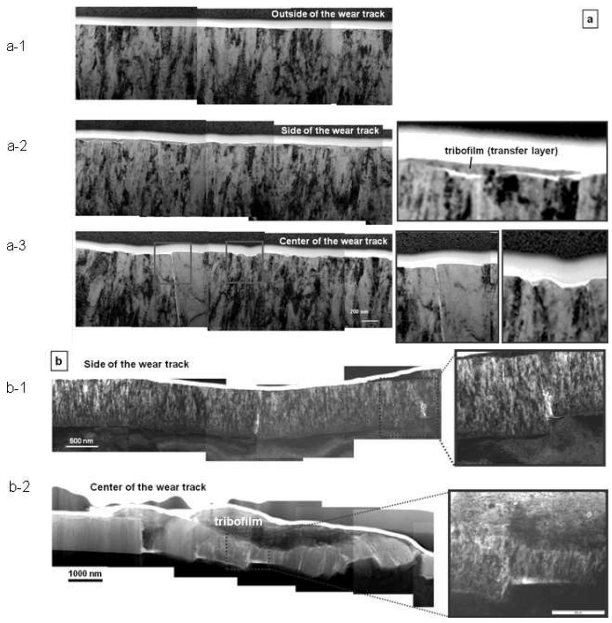

Fig. 18. TEM cross section micrographs from TiN single layer pin-on-disc wear tracks (a) under a load of 0.25 N after 10^4 cycles; a1 – outside of the wear track; a2 – side of the wear track; a3 – center of the wear track; (b) under a load of 1 N after 2×10^3 cycles; b1 – side of the wear track; b2 – center of the wear track

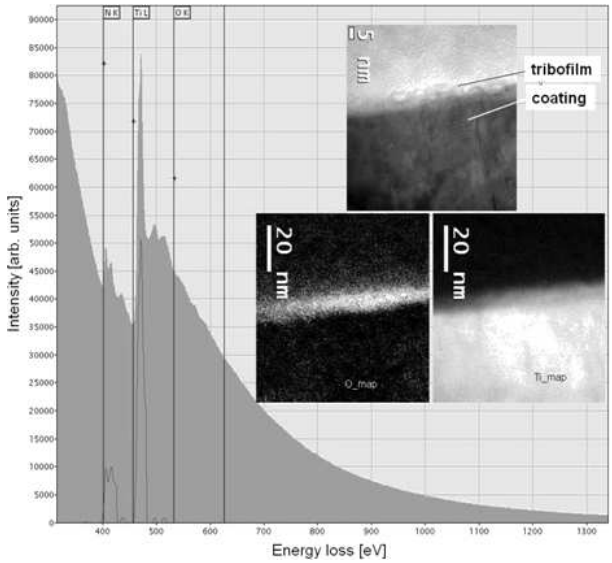

Fig. 19. Chemical analysis of the tribo-film (transfer layer) shown in Fig. 18a by an electron energy loss spectroscopy (EELS)

Fig. 20. a) TEM cross-section micrographs from the centre of a pin-on-disc wear track of the 4 bilayer Ti/TiN multilayer coating under a load of 1 N after 2×10^3 cycles and b) a fracture detail of the TiN layer in the contact zone

5. Conclusions

The deformation resistance of 1 μm thick Ti/TiN multilayer coatings consisting of bilayers of different modulation periods and different modulation ratios TiN:Ti magnetron sputtered on soft austenite steel substrates was investigated and compared to the resistance of single layer TiN coatings and correlated with mechanical and tribological properties of the coatings. The following conclusions have been drawn from this study:

1. The deposited TiN single layer coatings are characteristic of a high stress level, resulting in microcracks in the columnar growth structures. The stress level in the multilayer coatings is much lower and no fracture was observed in the as-deposited layers.
2. The hardness of the 16 bilayer coating with a bilayer period of 62 nm is the highest from all the coatings with a 1:1 modulation ratio. This result can be due to the Hall-Petch strengthening mechanism. Higher hardness could be reached for a lower metal content (i.e., for a higher TiN:Ti ratio).
3. Spherical indentation results in ring-like cracks around the indents for the TiN single layer coatings, while edge-like cracks and deformation, formed by shear deformation of Ti layers and brittle fracture of the TiN layers, are found in multilayer coatings. Shear steps are commonly found in the soft austenite substrate below these cracks or deformation bands. The deformation bands and cracks itself adapt their formation angle to the ratio of the brittle to soft phase (TiN:Ti). The higher the TiN content at higher modulation ratios, the more perpendicular to the coating surface are the deformation bands and cracks.
4. Adhesion strength was found to be high for multilayer coatings with TiN:Ti ratio 2:1 and 4:1, while for the coatings with the modulation ratio 1:1 the critical adhesion LC2 is much less. Too low bilayer periods (e.g., for 32 bilayers) have detrimental effects on the adhesion, hardness and wear resistance due to loss of multilayer structure and Hall-Petch strengthening.
5. Wear reduction can be achieved with multilayers of TiN:Ti ratio 2:1 and 4:1. In addition to good adhesion and hardness results, the multilayer coatings have high wear resistance and showed a layer-by-layer wear mechanism. In contrast to that, the single TiN layers do not survive wear testing against alumina ball.

Acknowledgements. The financial support of this work by the:

– the research project of the National Science Centre, No: 3066/B/T02/2011/40;
– the Polish-Austrian exchange project PL 12/2010;
– Austrian Federal Ministry of Traffic, Innovation and Technology; the MNT-ERA.NET Programme are highly acknowledged.

REFERENCES

[1] H. Holleck and V. Schier, "Multilayer PVD coatings for wear protection", *Surf. Coat. Technol*. 76–77, 328–336 (1995).
[2] M. Nordin, M. Larsson, and S. Hogmark, "Mechanical and tribological properties of multilayered PVD TiN/CrN, TiN/MoN, TiN/NbN and TiN/TaN coatings on cemented carbide", *Surf. Coat. Technol*. 106, 234–241 (1998).
[3] A.A. Voevodin, J.M. Schneider, C. Rebholz, and A. Matthews, "Multilayer composite ceramic- metal- DLC coatings for sliding wear applications", *Tribol. Int.* 29, 559–570 (1996).
[4] M. Stueber, H. Holleck, H. Leiste, K. Seemann, S. Ulrich, and C. Ziebert, "Concepts for the design of advanced nanoscale PVD multilayer protective thin films", *J. Alloys and Compounds* 483, 321- 333 (2009).
[5] E. Martinez, J. Romero, A. Lousa, and J. Esteve, "Nanoindentation stress-strain curves as a method for thin-film complete mechanical characterization: application to nanometric CrN/Cr multilayer coatings", *Appl. Phys*. A 77, 419–426 (2003).
[6] J. Smolik and K. Zdunek, "Effect of interlayer composition on the tribological properties of TiC/Ti(C_x, N_{1-x})/TiN antiabrasive multi-layer coatings", *Vacuum* 55, 147–151 (1999).
[7] Y.L. Su and W.H. Kao, "Optimum multilayer TiN-TiCN coatings for wear resistance and actual application", *Wear* 223, 119–130 (1998).
[8] N. Dück, W. Gamer, M. Gesatzke, W. Griepentrog, M. Österle, I. Sahre, and Ž. Urban, "Ti/TiN multilayer coatings, deposition technique, characterization and mechanical properties", *Surf. Coat. Technol*. 142–144, 579–584 (2001).
[9] S. Labdi, Ph. Houdy, P. Psyllaki, and M. Jeandin, "Elaboration and characterization of Ti and TiN thin films and Ti/TiN multilayers for hard coating applications", *Thin Solid Films* 275, 213–215 (1996).
[10] M. Nordin, M. Larsson, and S. Hogmark, "Mechanical and tribological properties of multilayered PVD TiNrCrN", *Wear* 232, 221–225 (1999).
[11] M. Nordin, M. Larsson, and S. Hogmark, "Wear resistance of multilayered PVD TiN/TaN on HSS", *Surf. Coat. Technol.* 120–121, 528–534 (1999).
[12] J. Smolik, K. Zdunek, and B. Larisch, "Investigation of adhesion between component layers of a multi-layer coating TiC/Ti(C_x, N_{1-x})/TiN by the scratch-test method", *Vacuum* 55, 45–50 (1999).
[13] M. Bromark, M. Larsson, P. Hedenqvist, and S. Hogmark, "Wear of PVD Ti/TiN multilayer coatings", *Surf. Coat. Technol.* 90, 217–223 (1997).
[14] A. Leyland and A. Matthews, "Thick Ti/TiN multilayered coatings for abrasive and erosive wear resistance", *Surf. Coat. Technol.* 70, 19–25 (1994).
[15] A. Matthews and S.S. Eskilden, "Engineering applications for diamond-like carbon", *Diamond Relat. Mater.* 3, 902–911 (1994).

[16] K. Holmberg, A. Matthews, and H. Ronkainen, "Coatings tribology–contact mechanics and surface design", *Tribol. Int.* 31 (1–3), 107–120 (1998).
[17] A. Matthews, R. Jones, and S. Dowey, "Modelling the deformation behaviour of multilayer coatings", *Tribology Letters* 11, 103–106 (2001).
[18] G.S.Kim, S.Y.Lee, J.H.Hahn, B.Y.Lee, J.G.Han, J.H.Lee, and S.Y.Lee, "Effects of the thickness of Ti buffer layer on the mechanical properties of TiN coatings", *Surf. Coat. Technol.* 171, 83–90 (2003).
[19] J.M. Lackner, "Industrially-scaled room-temperature pulsed laser deposition of Ti-TiN multilayer coatings", *J. Physics, Conf. Series* 59, 16–21 (2007).
[20] Z. Farhat, Y. Ding, D.O. Northwood, and A.T. Alpas, "Nanoindentation and friction studies on Ti-based nanolaminated films", *Surf. Coat. Technol*. 89, 24–30 (1997).
[21] S. Zhang and N. Ali, Nanocomposite *Thin Films and Coatings*, Imperial Colleage Press, London, 2007.
[22] A. Leyland and A. Matthews, "Thick Ti/TiN multilayered coatings for abrasive and erosive wear resistance", *Surf. Coat. Technol*. 70, 19–25 (1994).
[23] K. Holmberg, A. Matthews, and H. Ronkainen, "Coatings tribology – contact mechanisms and surface design", *Tribol. Intern.* 31, 107–120 (1998).
[24] K.S. Chan, M.Y. He, and J.W. Hutchinsson, "Cracking and stress redistribution in ceramic layered composites", *Mater. Sci. Eng.* 167, 57–64 (1993).
[25] M.Y. He and A.G. Evens, "Crack deflection at an interface between dissimilar elastic materials, role of residual stresses", *Int. J. Solids. Struct.* 31, 3443–3455 (1994).
[26] J.M. Lackner, *Industrially-scaled hybrid Pulsed Laser Deposition at Room Temperature*, Orekop, Kraków, 2006.
[27] W.C. Oliver and G.M. Pharr, "Piezoelectric nanoindentation", *J. Materials Research* 7, 1564–1583 (1992).
[28] A.C. Fischer-Cripps, "Critical review of analysis and interpretation of nanoindentation test data", *Surface and Coatings Technology* 200, 4153–4165 (2006).
[29] X.C. Zhang, B.S. Xu, H.D. Wang, and Y.X. Wu, "Hertzian contact response of single-layer, functionally graded and sandwich coatings", *Materials and Design* 28, 47–54 (2007).
[30] M.T. Tilbrook, D.J. Paton, Z. Xie, and M. Hoffman, "Microstructural effects on indentation failure mechanisms in TiN coatings, finite element simulations", *Acta Materialia* 55, 2489–2501 (2007).
[31] D.E. Vlachos, Y.P. Markopoulos, and V. Kostopoulos, "3-D modeling of nanoindentation experiment on a coating-substrate system", *Computational Mechanics* 27, 138–144 (2001).
[32] S.B. Liu, A. Peyronnel, Q.J. Wang, and L.M. Keer, "An extension of the Hertz theory for 2D coated components", *Tribology Letters* 18, 505–511 (2005).
[33] X.C. Zhang, B.S. Xu, H.D. Wang, Y.X. Wu, and Y. Jiang, "Hertzian contact response of single-layer, functionally graded and sandwich coatings", *Materials and Design* 28, 47–54 (2007).
[34] I. Pane and E. Blank, "Response to loading and stiffness of coated substrates indented by spheres", *Surface and Coatings Technology* 200, 1761–1767 (2005).
[35] M. Kot, "Deformations and fracture of coating-substrate systems under contact load", *Tribologia* 231, 125–134 (2010).
[36] B.R. Lawn, "Fracture and deformation in brittle solids, a perspective on the issue of scale", *J. Mater. Res.* 19, 22–29 (2004).
[37] B.R. Lawn and T.R. Wilshaw, "lndentation fracture: principles and applications", *J. Mater. Sci.* 10, 1049–1081 (1975).
[38] B.R. Lawn, Y. Deng, P. Miranda, A. Pajares, H. Chai, and D.K. Kim, "Overview: damage in brittle layer structures from concentrated loads", *J. Mater. Res*. 17, 3019–3036 (2002).
[39] H. Chai, B.R. Lawn, and S. Wuttiphan, "Fracture modes in brittle coatings with large interlayer modulus mismatch", *J. Mater. Res.* 14, 3805–3817 (1999).
[40] E. Weppelmann and M.V. Swain, "Investigation of the stresses and stress intensity factors responsible for fracture of thin protective films during ultra-micro indentation tests with spherical indenters", *Thin Solid Films* 286, 111–121 (1996).
[41] R. Anderson, G. Toth, L. Gan, and M.V. Swain, "Indentation response and cracking of sub-micron silica films on a polymeric substrate", *Eng. Fract. Mech*. 61, 93–105 (1998).
[42] H. Chai and B.R. Lawn, "Role of adhesive interlayer I transverse fracture of brittle layer structures", *J. Mater. Res.* 15, 1653–1660 (2000).
[43] A. Leyland and A. Matthews, "On the significance of the H/E ratio in wear control: a nanocomposite coating approach to optimised tribological behavior", *Wear* 246, 1–11 (2000).
[44] A. Matthews and A. Leyland, "Developments in PVD tribological coatings", *Proc. 5th ASM Heat Treatment and Surface Engineering Conf. Eur.* 1, CD-ROM (2000).
[45] K. Holmberg and A. Matthews, *Coatings Tribology, Properties, Techniques and Applications, Surface Engineering,* Elsevier, Amsterdam, 1996.
[46] K. Holmberg and A. Matthews, "Coatings tribology: a concept, critical aspects and future directions", *Thin Solid Films* 253, 173–178 (1994).
[47] A. Matthews, A. Leyland, K. Holmberg, and H. Ronkainen, "Design aspects for advanced tribological surface coatings", *Surf. Coat. Technol.* 100–101, 1–6 (1998).
[48] J. Michler and E. Blank, "Analysis of coating fracture and substrate plasticity induced by spherical indentors: diamond and diamond-like carbon layers on steel substrates", *Thin Solid Films* 381, 119–134 (2001).
[49] R.F. Bunshah, *Handbook of Hard Coating*, William Andrew Publishing, Norwich, 2001.
[50] S. Gwidon and W. Stachowiak, *Wear – Materials, Mechanisms and Practise,* Wiley, Chichester, 2005.
[51] J.M. Lackner, W. Waldhauser, A. Alamanou, C. Teichert, F. Schmied, L. Major, and B. Major, "Mechanisms for self-assembling topography formation in low-temperature vacuum deposition of inorganic coatings on polymer surfaces", *Bull. Pol. Ac.: Tech.* 58, 281–294 (2010).
[52] A. Lousa, J. Romero, E. Martinez, J. Esteve, F. Montala, and L. Carrera, "Multilayered chromium/chromium nitride coatings for use in pressure die-casting", *Surface and Coatings Technology* 146–147, 268–273 (2001).
[53] J. Romero, J. Esteve, and A. Lousa, "Period dependence of hardness and microstructure on nanometric Cr/CrN multilayers", *Surface and Coatings Technology* 188–189, 338–343 (2004).
[54] L. Maille, P. Aubert, C. Sant, and P. Garnier, "A mechanical study of W-N/W multilayers", *Surface and Coatings Technology* 180–181, 483–487 (2004).
[55] S.K. Kim, Y.J. Baik, and D. Kwon, "Analysis of interfacial strengthening from composite hardness of TiN/VN and TiN/NbN multilayer hard coatings", *Surface and Coatings Technology* 187, 47–53 (2004).

[56] G. Abadias, S. Dub, and R. Shmeger, "Nanoindentation hardness and structure of ion beam sputtered TiN, W and TiN/W multilayer hard coatings", *Surface and Coatings Technology* 200, 6538–6543 (2006).

[57] M. Berger, U. Wiklund, M. Eriksson, H. Engqvist, and S. Jacobson, "The multilayer effect in abrasion – optimising the combination of hard and tough phases", *Surface and Coatings Technology* 116–119, 1138–1144 (1999).

[58] M. Kot, W.A. Rakowski, Ł. Major , R. Major, and J. Morgiel, "Effect of bilayer period on properties of Cr/CrN multilayer coatings produced by laser ablation", *Surface and Coatings Technology* 202, 3501–3506 (2008).

[59] S.K. Tien and J.G. Duh, "Effect of heat treatment on mechanical properties and microstructure of CrN/AlN multilayer coatings", *Thin Solid Films* 494, 173–178 (2006).

[60] G.S. Kim, S.Y. Lee, and J.H. Hahn, "Synthesis of CrN/AlN superlattice coatings using closed-field unbalanced magnetron sputtering process", *Surf. Coat. Technol*. 171, 91–95 (2003).

[61] A. Dück, N. Gamer, W. Gesatzke, M. Griepentrog, W. Österle, M. Sahre, and I. Urban, "Ti/TiN multilayer coatings: deposition technique, characterization and mechanical properties", *Surf. Coat. Technol*. 142–144, 579–584 (2001).

[62] E.O. Hall, "The deformation and ageing of mild steel", *lst Proc. Physics Society III Discussion of Results* B 64, 747–753 (1951).

[63] S.L. Lehoczky, "Retardation of dislocation generation and motion in thin-layered metal laminates", *Review Letter* 41, 1814–1819 (1978).

[64] M.T. Vieira and A.S. Ramos, "The influence of ductile interlayers on the mechanical performance of tungsten nitride coatings", *J. Materials Processing Technology* 92–93, 156–161 (1999).

[65] E. Bemporad, M. Sebastiani, C. Pecchio, and S. De Rossi, "High thickness Ti/TiN multilayer thin coatings for wear resistant applications", *Surface and Coatings Technology* 201, 2155–2165 (2006).

[66] A. Leyland and A. Matthews, "Design criteria for wear-resistant nanostructured and glassy-metal coatings", *Surf. Coat. Technol*. 177–178, 317–324 (2004).

[67] T.Y. Tsui, G.M. Pharr, W.C. Oliver, C.S. Bhatia, R.L. White, S. Anders, A. Anders, and I.G. Brown, "Nanoindentation and nanoscratching of hard carbon coatings for magnetic disks mater", *Res. Soc. Symp. Proc.* 383, 447–452 (1995).

[68] J. Musil, "Hard and superhard nanocomposite coatings", *Surface and Coatings Technology* 125, 322–330 (2000).

[69] Y.T. Pei, P. Huizenga, D. Galvan, and J.Th.M. De Hossona, "Self-lubrication and wear behavior of TiC/a-C:H nanocomposite coatings", *J.. Appl. Phys*. 100, 114309–114318 (2006).

[70] A. Karimi, Y. Wang, T. Cselle, and M. Morstein, "Fracture mechanisms in nanoscale layered hard thin films", *Thin Solid Films* 420–421, 275–280 (2002).

[71] J.W. Hutchinson, M.D. Thouless, and E.G. Liniger, "Growth and configurational stability of circular, buckling-driven film delaminations", *Acta Metall.* 40, 295–308 (1992).

[72] M. Kot, L. Major, J.M. Lackner, and W. Rakowski, "Analysis of the influence of sublayer thickness on the deformation mechanism and fracture of {Ti/TiN} multilayer", *Tribology* 232, 181–189 (2010).

[73] M. Kot, W. Rakowski, J. Morgiel, and L. Major, "Deformation of coating-substrate systems under contact load", *Tribology* 218, 285–295 (2008).

[74] E.G. Herbert, G.M. Pharr, W.C. Oliver, B.N. Lucas, and J.L. Hay," On the measurement of stress–strain curves by spherical indentation", *Thin Solid Films* 398–399, 331–335 (2001).

[75] N.J.M. Carvalho and J.Th.M. De Hosson, "Deformation mechanisms in TiN/(Ti,Al)N multilayers under depth-sensing indentation", *Acta Materialia* 54, 1857–1862 (2006).

[76] M. Oden, H. Ljungcrantz, and L. Hultman, "Characterization of the induced plastic zone in a single crystal TiN(001) film by nanoindentation and transmission electron microscopy", *J. Mater. Res.* 12, 2134–2142 (1997).

[77] T. Hayashi and S.Mukamel, "Multidimensional infrared signatures of intramolecular hydrogen-bonding in malonaldehyde", *J.Phys.Chem.* 1079, 113–9131 (2003).

[78] J.-K. Park, C. Ziebert, M. Stüber, and Y.-J. Baik, "Improvement of hardness and toughness of TiAlN coating by nanoscale multilayered structurization with Si_3N_4, *Plasma Process. Polym*. 4, 902–905 (2007).

[79] Z.H. Xie, M. Hoffman, P. Munroe, A. Bendavid, and P.J. Martin, "Deformation mechanisms of TiN multilayer coatings alternated by ductile or stiff interlayers", *Acta Materialia* 56, 852–861 (2008).

[80] K.J. Ma, A. Bloyce, and T. Bell, "Examination of mechanical properties and failure mechanisms of TiN and Ti-TiN multilayer coatings", *Surf. Coat. Technol*. 76–77, 297–302 (1995).

[81] R. Hübler, G.K. Wolf, W.H. Schreiner, and I.J.R. Baumvol," Ion beam mixing of Al–AlN multilayers for tribological and corrosion protection", *Nuc. Inst. Met. Phy. Res*. B 80–81, 1415–1418 (1993).

[82] E. Martinez, J. Romero, A. Lousa, and J. Esteve, "Wear behavior of nanometric CrN/Cr multilayers", *Surface and Coatings Technology* 163–164, 571–577 (2003).